THERMAL DRIFT IN AN INCLINED VISCOUS FLUID FLOW

***Miloš M. JOVANOVIĆ*[*1], Saša M. MILANOVIĆ[1], Živan T. SPASIĆ[1]**

[1] University of Niš, Faculty of Mechanical Engineering, Niš, Serbia

[*] Corresponding author; E-mail: milos.jovanovic@masfak.ni.ac.rs

This paper considers viscous fluid flow in a slot between two parallel plates which start inclining with respect to the horizontal line. The lower plate was heated and had nonhomogeneous temperature distribution while the upper plate was cooled and with homogeneous temperature distribution. The spatially periodic temperature distribution was gradually applied at the lower plate, after which the plates were slowly inclined in the positive-counterclockwise direction, and the fields of vorticity, streamfunction and temperature are pesented for different values of the angle of inclination. We used the vorticity-streamfunction formulation of Navier-Stokes equations, Fourier-Galerkin and Chebyshev collocation method for numerical simulation of 2D viscous fluid flow. We carried out numerical simulation using our in-house Matlab code for subcritical uniform Rayleigh number $\mathrm{Ra}_{\mathrm{uni}}$*, and periodic Rayleigh number* Ra_{p} *on the lower plate. An accurate numerical scheme was developed to capture the full time-dependent behavior here. The interest lied in how the intensities of the vortexes and convection rolls changed as the inclination angle was increased with respect to time. Convection rolls rotating in the clockwise direction expanded and the rolls rotating in the counterclockwise direction shrank and their centers moved closer to the lower wall. Thermal drift appeared between them when the inclination angle started increasing.*

Key words*:Boussinesq approximation, Spectral method, thermal drift.*

1. Introduction

Natural convection is among the most frequently occurring forms of viscous fluid motion. A commonly found issue in natural convection is when flow in a horizontal slot is subjected to a spatially homogeneous heating that is applied at the lower plate. This issue is known as Rayleigh-Bénard convection (RBC) [1], [2]. It has been studied for many years using different approaches [3]. Convection comes as a consequence of the transition from a conductive state that occurs when critical conditions are exceeded [4] and it changes the character of heat flow in qualitative terms. These critical conditions are expressed in terms of the critical Rayleigh number Ra_{cr}, with changes in flow occurring when $Ra > Ra_{cr}$ at a given wave number. In the other hand temperature non-uniformities form horizontal and vertical temperature gradients which in turn lead to horizontal density variations, creating motions often referred to as horizontal convection.

Optimal heat transfer was studied in [5]. More intense heating results in secondary bifurcations in three-dimensional fluid flows and the onset of different types of instability were analyzed in [6],[7], described by using the so-called Busse balloon. A sufficiently large heating intensity causes turbulent

RBC [8-10]. Several studies have examined the effects of geometric non-uniformities on such convections [11].

Onset conditions can be affected by inhomogeneous temperature distribution in the plate geometry [12-14]. There is no state with conduction only that can exist in the presence of geometric modulations, meaning that natural convection will sets in regardless of the heating intensity [15]. Temperatures non-uniformities also affect the onset conditions [16], and can create their own convection, which once again appears regardless of the heating intensity [17-21]. The buoyancy driven recirculating flows within enclosures non-uniformly heated from either the top or the bottom surface constitute commonly-investigated classical problems [22-28].

The numerical analyses focused on convection in an infinite vertical slot which has one wall with a corrugated profile, and which is subject to either uniform or periodic heating was published in [29]. In [30] it was numerically shown that horizontal convection may be unsteady and turbulent, possessing the capability of preserving the overturning circulation within a layer. Bearing in mind that the response of a system depends on the Prandtl number [31], we focus our discussion on water $(\mathrm{Pr}=7)$. The fields of vorticity and the equation time dependancy are often omitted in literature for patterned heating, since there are no known boundary conditions for vorticity at the plates, and they have to be computed as part of the solution. We used the influence matrix method to circumvent this problem [32]. Inclined slots are of interest in the development of energy efficient ventilation systems, passive cooling devices, in predicting fire propagation and in removing smoke from structures, as presented in [33] and in references therein.

Periodic heating applied to smooth channels in the absence of any mean pressure gradient results in the formation of a system of pairs of counter rotating rolls regardless of whether the heating is applied at the lower, upper, or both plates,[19-21] and there is no net horizontal flow. The addition of grooves to such channels produces a net horizontal flow in the direction transverse to the grooves because of the creation of thermal drift whose strength and direction depend on the relative position of the groove and heating patterns. In this paper we will show that the inclination of the slot can cause the fluid temperature pattern to move due to buoyancy and the gravity component in the *x*-taxis direction, and that the phase shift between fluid temperature pattern tips and hot spots on the lower plate can cause a stream tube. Structured convection, which results from the use of spatial heating patterns, possesses some interesting properties. It has been extensively studied in horizontal slots, but scarce information is available about inclined slots [33].

2. Mathematical model

We consider viscous fluid flow resulting from natural convection in a fluid layer in an infinite slot bounded by solid walls which are inclined with respect to the horizontal line. The lower wall temperature consists of two components-homogeneous temperature T_{w2} and spatially periodic temperature $T_p(x)$, and the upper isothermal wall only has the homogeneous part T_{w1}, where $T_{w2}>T_{w1}$. The heating produces a cosinusoidal temperature variation along the x-direction characterized by the wave number α with the amplitude expressed in terms of the periodic temperature $T_p(x)$.

The equations that describe the viscous, Newtonian fluid flow and heat transfer read,

$$\frac{\partial\vec{\omega}}{\partial t}+\vec{v}\cdot\nabla\vec{\omega}=\nabla\times\vec{F}+\nu\Delta\vec{\omega}, \qquad \vec{\omega}+\Delta\vec{\psi}=0, \qquad \frac{\partial T}{\partial t}+\vec{v}\cdot\nabla T=\frac{\lambda_f}{\rho c_p}\Delta T+\dot{q}, \tag{1,2,3}$$

with appropriate boundary conditions:

$$y = H/2, \quad \psi = \int_{-1}^{1} u(y)dy, \ \frac{\partial \psi}{\partial y} = 0, \ T = T_{w1},$$
$$y = -H/2, \quad \psi = 0, \ \frac{\partial \psi}{\partial y} = 0, \ T = T_{w2} + \frac{1}{2}T_p \cos(\alpha x + \varphi). \tag{4}$$

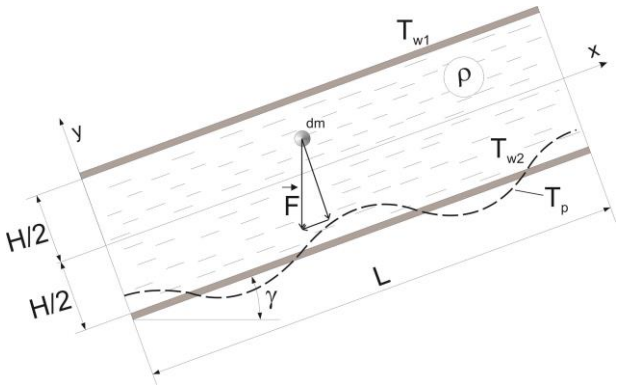

Figure 1. Physical model

There is no externally imposed horizontal pressure gradient, i.e. $\partial p/\partial x = 0$. The boundary conditions for vorticity are not known and have to be computed as a part of the numerical solution. For this purpose, we apply the influence matrix method which can be applied for such problems [32]. We use equation $\vec{\omega} = \nabla \times \vec{v}$ (2) instead of continuity equation $\nabla \cdot \vec{v} = \nabla \cdot (\nabla \times \vec{\psi}) \equiv 0$ which is satisfied identically in the vorticity-streamfunction $(\omega - \psi)$ formulation of the Navier-Stokes equation, so for closing the system of equations we use $\vec{\omega} = \nabla \times \vec{v}$, $\vec{v} = \nabla \times \vec{\psi}$, $\vec{\psi} = \psi \vec{k}$, to get equation (2). In the previous equation (1)-(3) we used the following notations: $\vec{v}$ - fluid velocity vector, $\vec{\omega}$ - fluid vorticity vector, $\vec{F}$ - volumetric force per unit mass, $\vec{\psi}$ - streamfunction vector, T - temperature of the fluid, ν - kinematic viscosity (momentum diffusivity), $\kappa = \lambda_f / \rho c_p$ - thermal diffusivity, λ_f -fluid thermal conductivity, ρ - fluid density, c_p - specific heat at constant pressure, $\dot{q}$ - heat flux per unit volume, $\Delta = \nabla \cdot \nabla$ -Laplacian of scalar or vector field, as a dot product of nabla operator ∇ with itself. In fig.1 H -distance between the parallel plates, L - length of the periodic slot filled with the viscous fluid, T_{w1} - temperature of the upper colder plate, T_{w2} - homogeneous part of the temperature of lower warmer plate, T_p - peak to peak amplitude of the periodic temperature at the lower plate, α - wave number of periodic temperature, φ- phase shift of periodic temperature on the lower wall.

In the Boussinesq approximation density changes only in the force term in the momentum equation according to $V = V_0[1 + \beta(T - T_0)]$ where β - is the thermal expansion coefficient, where $\beta = 1/T \sim 3 \cdot 10^{-3} \mathrm{K}^{-1}$ for gases, and $\beta = 1/T \sim 5 \cdot 10^{-4} \mathrm{K}^{-1}$ for liquids, so we have the following relationship (5) for *m*=const. After substituting (5) into the force term of vorticity transport equation (6), which only takes into account the fluid density variations, we obtain

$$\frac{\rho - \rho_0}{\rho_0} = \frac{-\beta(T - T_0)}{1 + \beta(T - T_0)} \approx -\beta(T - T_0), \tag{5}$$

$$\vec{F} = \frac{\rho}{\rho_0} g(-\sin\gamma \vec{i} - \cos\gamma \vec{j}) \approx [1 - \beta(T - T_0)] g(-\sin\gamma \vec{i} - \cos\gamma \vec{j}). \tag{6}$$

Here we have anticipated $T_0 = T_{w1}$ and that the plates can be parallel to each other but with some inclination angle γ with respect to the horizontal line. The results of numerical simulation in this paper are displayed for different angles of inclinations *x* and *y* are the longitudinal and transverse coordinate and *g*-the gravitational acceleration. In order to obtain the nondimensional form of the previous equations, we choose the length scales $L/2\pi$ and *H/2* in the direction of the *x*- and the *y*- axis respectively, in accordance with the domain of basic functions, using the Fourier expansion in the *x*-

axis direction and the Chebyshev expansion in the *y*-axis direction., so that the following length, time, vorticity and streamfunction scales are

$$\psi = \kappa\psi^*, \quad \omega = \frac{\kappa}{H^2}\omega^*, \quad t = \frac{H^2}{\kappa}t^*, \quad T^* = \frac{T - T_{w1}}{T_{w2} - T_{w1}}, \quad T_p^* = \frac{T_p}{T_{w2} - T_{w1}},$$
$$x = \frac{L}{2\pi}x^*, \ \left(0 \le x^* \le 2\pi\right), \quad y = \frac{H}{2}y^*, \ \left(-1 \le y^* \le 1\right). \tag{7}$$

The field equations, which consist of vorticity transport equation (1), the definition of vorticity instead of continuity equation (2) and thermal energy transport equation (3), now have the following nondimensional form

$$\frac{\partial\omega^*}{\partial t^*} + 4a\left(\frac{\partial\psi^*}{\partial y^*}\frac{\partial\omega^*}{\partial x^*} - \frac{\partial\psi^*}{\partial x^*}\frac{\partial\omega^*}{\partial y^*}\right) = 2Ra\,\mathrm{Pr}\left(a\frac{\partial T^*}{\partial x^*}\cos\gamma - \frac{\partial T^*}{\partial y^*}\sin\gamma\right) + 4\,\mathrm{Pr}\left(a^2\frac{\partial^2\omega^*}{\partial x^{*2}} + \frac{\partial^2\omega^*}{\partial y^{*2}}\right), \tag{8}$$

$$\omega^* + 4\left(a^2\frac{\partial^2\psi^*}{\partial x^{*2}} + \frac{\partial^2\psi^*}{\partial y^{*2}}\right) = 0, \quad \frac{\partial T^*}{\partial t^*} + 4a\left(\frac{\partial\psi^*}{\partial y^*}\frac{\partial T^*}{\partial x^*} - \frac{\partial\psi^*}{\partial x^*}\frac{\partial T^*}{\partial y^*}\right) = 4\left(a^2\frac{\partial^2 T^*}{\partial x^{*2}} + \frac{\partial^2 T^*}{\partial y^{*2}}\right) + q^*, \tag{9,10}$$

where we use the following nondimensional parameters,

$$Ra_{uni} = \frac{g\beta\left(T_{w2} - T_{w1}\right)H^3}{\kappa\nu}, \quad Ra_p = \frac{g\beta T_p H^3}{\kappa\nu}, \quad a = \frac{\pi H}{L}, \quad \mathrm{Pr} = \frac{\nu}{\kappa}, \quad \kappa = \frac{\lambda_f}{\rho c_p}. \tag{11}$$

In the expressions above Ra_{uni} and Ra_p represent the uniform and periodic Rayleigh numbers measuring the intensity of the uniform and periodic heating component, a is aspect ratio of vertical to horizontal slot dimensions, and Pr is the Prandtl number as a ratio of the momentum diffusivity ν to thermal diffusivity κ. The initial and boundary conditions in the nondimensional form are as follows:

$$t^* = 0, \quad \psi^*\left(x^*, y^*\right) = 0, \quad \omega^*\left(x^*, y^*\right) = 0, \quad T^*\left(x^*, y^*\right) = \frac{1}{2}\left(1 - y^*\right), \quad T_p^* = T_p/\left(T_{w2} - T_{w1}\right),$$
$$y^* = 1, \quad \psi^* = \int_{-1}^{1} u^*\left(y^*\right)dy^*, \quad \frac{\partial\psi^*}{\partial y^*} = 0, \quad T^* = 0, \quad 0 < t^* \le \pi,$$
$$y^* = -1, \quad \psi^* = 0, \quad \frac{\partial\psi^*}{\partial y^*} = 0, \quad T^* = 1 + \frac{1}{2}T_p^*\left(t^*\right)\cos\left(\alpha x^* + \varphi\right), \quad 0 < t^* \le \frac{\pi}{2}. \tag{12}$$

For the starting value we use the flow rate for the flow between two plates with homogeneous temperatures without a temperature difference between them

$$y^* = 1, \quad \psi^* = \int_{-1}^{1} u^*\left(y^*\right)dy^* = \int_{-1}^{1} -\frac{g\sin\gamma}{\nu}\frac{H^3}{4\kappa}\left(1 - 2y^* - y^{*2}\right)dy^* = -\frac{4}{3}\frac{H^3}{\kappa}\frac{g\sin\gamma}{\nu}, \tag{12b}$$

and later this value is calculated using the Chebyshev approximation of the Fourier coefficient based on the Gauss quadrature formula

$$y^* = 1, \quad \psi^* = \int_{-1}^{1} u^*\left(y^*\right)dy^* = \int_{-1}^{1} \hat{u}_0^{n+1}\left(y^*\right)dy^* = \sum_{\substack{m=0 \\ m \text{ even}}}^{N_y} \frac{2}{m^2 - 1}\tilde{u}_{0,m}^{n+1}. \tag{12c}$$

In order to achieve such a numerical simulation, we use the four time-level, third order temporal discretization procedure AB/BDI3 [34, p.51]. This semi-implicit method applies generally to nonlinear equations such as (8) and (10) where the coefficients of the linear operator are constant. The details of the spatial and time discretization procedure were described in [35].

3. The Numerical Procedure

Equations (8), (9) and (10) with boundary and initial conditions (12) should be numerically solved with an appropriate procedure. For the numerical simulation we use our pseudo-spectral code,

developed in MATLAB. For the direction of the plates (x-axis) we use the Fourier-Galerkin method, and for the approximation in the normal direction (y-axis) we used Chebyshev collocation method. The dependant variables are expressed in terms of trigonometric polynomials in the following way:

$$\chi_N^*\left(x^*,y^*,t^*\right)=\sum_{k=-N_x/2}^{k=N_x/2}\hat{\chi}_k\left(y^*,t^*\right)e^{\underline{i}kx^*}. \tag{13}$$

Here χ represents either the nondimensional vorticity, streamfunction or temperature, $\chi_N^*\left(x^*,y^*,t^*\right)=\omega^*,\psi^*,T^*$. In the expression above $\underline{i}=\sqrt{-1}$ is the imaginary unit, k-wave number, $\hat{\omega}_k\left(y^*,t^*\right)$, $\hat{\psi}_k\left(y^*,t^*\right)$, and $\hat{\theta}_k\left(y^*,t^*\right)$ are the Fourier coefficients for dimensionless vorticity, stream function and temperature respectively and $\left\{\hat{\omega}_k\left(y^*,t^*\right),\hat{\psi}_k\left(y^*,t^*\right),\hat{\theta}_k\left(y^*,t^*\right)\right\}\in \mathrm{X}$, i.e. they are all complex numbers. For advective (nonlinear) terms on the left hand side of the transport equations of vorticity (8) and thermal energy (10) we use these discrete inverse Fourier transformations

$$N_{\chi 1}=\sum_{k=-N_x/2}^{k=N_x/2}\hat{N}_{\chi 1,k}\left(y^*,t^*\right)e^{\underline{i}kx^*}=\sum_{k=-N_x/2}^{N_x/2}\left[\widehat{\frac{\partial\psi^*}{\partial y^*}\frac{\partial\chi}{\partial x^*}}\right]_k\left(y^*,t^*\right)e^{\underline{i}kx^*}, \tag{14}$$

$$N_{\chi 2}=\sum_{k=-N_x/2}^{k=N_x/2}\hat{N}_{\chi 2,k}\left(y^*,t^*\right)e^{\underline{i}kx^*}=\sum_{k=-N_x/2}^{N_x/2}\left[\widehat{\frac{\partial\psi^*}{\partial x^*}\frac{\partial\chi}{\partial y^*}}\right]_k\left(y^*,t^*\right)e^{\underline{i}kx^*},\ \chi=\omega^*,\theta^*. \tag{15}$$

If we substitute these trigonometric polynomials (13-15) into equations (8),(9) and (10), and use the orthogonality condition for basic functions in this case, which reads

$$\left\langle e^{\underline{i}kx^*},e^{\underline{i}lx^*}\right\rangle=\int_0^{2\pi}e^{\underline{i}kx^*}e^{\underline{i}lx^*}dx=\begin{cases}2\pi, l=k\\ 0,\ \ l\neq k\end{cases} \tag{16}$$

the following system of equations is obtained, and if we drop $*$ for the nondimensional notation,

$$\frac{\partial\hat{\omega}_k}{\partial t}(y,t)+4a\left[\widehat{\frac{\partial\psi}{\partial y}\frac{\partial\omega}{\partial x}-\frac{\partial\psi}{\partial x}\frac{\partial\omega}{\partial y}}\right]_k-2\,\mathrm{Pr}\,\mathrm{Ra}\left(a\underline{i}k\cos\gamma\hat{\theta}_k-\sin\gamma\frac{\partial\hat{\theta}_k}{\partial y}\right)-4\,\mathrm{Pr}\left(a^2\left(\underline{i}k\right)^2\hat{\omega}_k+\frac{\partial^2\hat{\omega}_k}{\partial y^2}\right)=0, \tag{17}$$

$$\hat{\omega}_k\left(y,t\right)+4\left[a^2\left(\underline{i}k\right)^2\hat{\psi}_k\left(y,t\right)+\frac{\partial^2\hat{\psi}_k}{\partial y^2}(y,t)\right]=0,\quad l=k=0,1,...,K. \tag{18}$$

$$\frac{\partial\hat{\theta}_k}{\partial t}(y,t)+4a\left[\widehat{\frac{\partial\psi}{\partial y}\frac{\partial\theta}{\partial x}-\frac{\partial\psi}{\partial x}\frac{\partial\theta}{\partial y}}\right]_k(y,t)-4\left(a^2\left(\underline{i}k\right)^2+\frac{\partial^2}{\partial y^2}\right)\hat{\theta}_k(y,t)-\hat{q}_k(y,t)=0,\ l=k=0,1,...K. \tag{19}$$

then we get a system of equations, for the Fourier coefficients for vorticity $\hat{\omega}_k(y,t)$, stream function $\hat{\psi}_k(y,t)$ and temperature $\hat{\theta}_k(y,t)$, for each wavenumber from $k=1,...K$, where $K=N_x/2$, and N_x is the number of equispaced nodes on the x-axis. For discretization in the direction of the y-axis we use the Chebyshev collocation method, which consists of approximating the Fourier coefficients, used for the approximation in the x-axis direction, and the Chebyshev polynomials in the y-axis direction. The residuum obtained by substituting the Chebyshev polynomials in equations (17), (18), (19) is zero in Gauss-Lobatto-Chebyshev collocation points defined by $y_j=\cos\left(\pi j/N_y\right)$ for $j=0,1,...,N_y$, so the previous system of equations obtains the following form

$$\frac{\partial\hat{\omega}_{kN}}{\partial t}\left(y_j,t\right)+4a\left[\widehat{\frac{\partial\psi}{\partial y}\frac{\partial\omega}{\partial x}-\frac{\partial\psi}{\partial x}\frac{\partial\omega}{\partial y}}\right]_{kN}\left(y_j,t\right)-2\,\mathrm{Pr}\,\mathrm{Ra}\left(a\underline{i}k\cos\gamma\hat{\theta}_{kN}\left(y_j,t\right)+\sin\gamma\sum_{l=0}^{N_y}d_{j,l}^{(1)}\hat{\theta}_{kN}\left(y_l,t\right)\right)-$$

$$-4\,\mathrm{Pr}\left(a^2\left(\underline{i}k\right)^2\hat{\omega}_{kN}\left(y_j,t\right)\sum_{l=0}^{N_y}d_{j,l}^{(2)}\hat{\omega}_{kN}\left(y_l,t\right)\right)=0,\quad k=0,1,...N_x/2,\ \ j=0,1,...,N_y. \tag{20}$$

$$\hat{\omega}_{kN}\left(y_j,t\right)-4a^2k^2\hat{\psi}_{kN}\left(y_j,t\right)+4\sum_{l=0}^{N_y}d_{j,l}^{(2)}\hat{\psi}_{kN}\left(y_l,t\right)=0,\ \ k=0,1,...,N_x/2,\ \ j=0,1,...,N_y. \tag{21}$$

$$\frac{\partial \hat{\theta}_{kN}}{\partial t}\left(y_j,t\right)+4a\left[\widehat{\frac{\partial \psi}{\partial y}\frac{\partial \theta}{\partial x}}\right]_{kN}\left(y_j,t\right)+4a\left[\widehat{\frac{\partial \psi}{\partial x}\frac{\partial \theta}{\partial y}}\right]_{kN}\left(y_j,t\right)-4a^2\left(\underline{i}k\right)^2\hat{\theta}_{kN}\left(y_j,t\right)-$$

$$-4\sum_{l=0}^{N_y}d_{j,l}^{(2)}\hat{\theta}_{kN}\left(y_l,t\right)-\hat{q}_{kN}\left(y_j,t\right)=0,\ k=0,1,...N_x/2,\ j=0,1,...,N_y. \tag{22}$$

In this system of equations $\hat{\omega}_{kN}\left(y_j,t\right)$, $\hat{\psi}_{kN}\left(y_j,t\right)$, $\hat{\theta}_{kN}\left(y_j,t\right)$ represent the Chebyshev approximation of the corresponding Fourier coefficients $\hat{\omega}_k(y,t)$ $\hat{\psi}_k(y,t)$ $\hat{\theta}_k(y,t)$, and since in the Chebyshev collocation method we have $\hat{\omega}_k\left(y_j,t\right)=\hat{\omega}_{kN}\left(y_j,t\right)$, $\hat{\psi}_{kN}\left(y_j,t\right)=\hat{\psi}_k\left(y_j,t\right)$, $\hat{\theta}_{kN}\left(y_j,t\right)=\hat{\theta}_k\left(y_j,t\right)$ in Gauss-Lobatto-Chebishev nodes. In previous equations we used the elements of Chebyshev differentiation matrices $d_{j,l}^{(1)}$ - first order derivative, $d_{j,l}^{(2)}$ - second order derivative, given for the same nodes, whose expression can be found in [35,p.89]. The system of equations that should be solved by some time discretization scheme reads as:

$$\frac{\partial}{\partial t}\hat{\Omega}_k\left(t\right)+4a\left(\hat{\mathrm{N}}_{\omega 1,k}\left(t\right)+\hat{\mathrm{N}}_{\omega 2,k}\left(t\right)\right)=2\,\mathrm{Pr}\,\mathrm{Ra}\left(a\cos\gamma\,\underline{i}k\,\mathrm{I}_1+\sin\gamma\mathrm{D}_1\right)\hat{\Theta}_k\left(t\right)+$$

$$+4\,\mathrm{Pr}\left(a^2\left(\underline{i}k\right)^2\mathrm{I}_1+\mathrm{D}_2\right)\hat{\Omega}_k\left(t\right),\qquad k=0,1,...,N_x/2. \tag{23}$$

$$\hat{\Omega}_k\left(t\right)+4\left(a^2\left(\underline{i}k\right)^2\mathrm{I}_1+\mathrm{D}_2\right)\hat{\Psi}_k\left(t\right)=\mathbf{0}_1,\qquad k=0,1,...,N_x/2, \tag{24}$$

$$\frac{\partial\hat{\Theta}_k\left(t\right)}{\partial t}+4a\left(\hat{\mathrm{N}}_{\theta 1,k}\left(t\right)+\hat{\mathrm{N}}_{\theta 2,k}\left(t\right)\right)=4\left(a^2\left(\underline{i}k\right)^2\mathrm{I}_1+\mathrm{D}_2\right)\hat{\Theta}_k\left(t\right)+\hat{Q}_k\left(t\right),k=0,1,...,K, \tag{25}$$

$$\begin{aligned}
&\hat{\psi}_{kN}\left(y_0,t\right)=\hat{g}_{\psi+,k}\left(t\right),\quad \frac{\partial\hat{\psi}_{kN}}{\partial y}\left(y_0,t\right)=\sum_{l=0}^{N_y}d_{0,l}^{(1)}\hat{\psi}_{kN}\left(y_l,t\right)=\hat{h}_{\psi+,k}\left(t\right),\\
&\hat{\psi}_{kN}\left(y_{N_y},t\right)=\hat{g}_{\psi-,k}\left(t\right),\quad \frac{\partial\hat{\psi}_{kN}}{\partial y}\left(y_{N_y},t\right)=\sum_{l=0}^{N_y}d_{N_y,l}^{(1)}\hat{\psi}_{kN}\left(y_l,t\right)=\hat{h}_{\psi-,k}\left(t\right),
\end{aligned} \tag{26}$$

$$\begin{aligned}
&\hat{\theta}_{kN}\left(y_0,t\right)=\hat{g}_{\theta+,k}\left(t\right),\quad \frac{\partial\hat{\theta}_{kN}}{\partial y}\left(y_0,t\right)=\sum_{l=0}^{N_y}d_{0,l}^{(1)}\hat{\theta}_{kN}\left(y_l,t\right)=\hat{h}_{\theta+,k}\left(t\right),\\
&\hat{\theta}_{kN}\left(y_{N_y},t\right)=\hat{g}_{\theta-,k}\left(t\right),\quad \frac{\partial\hat{\theta}_{kN}}{\partial y}\left(y_{N_y},t\right)=\sum_{l=0}^{N_y}d_{N_y,l}^{(1)}\hat{\theta}_{kN}\left(y_l,t\right)=\hat{h}_{\theta-,k}\left(t\right).
\end{aligned} \tag{27}$$

In the equations above, all column matrices $\hat{\Psi}_k(t)$, $\hat{\Omega}_k(t)$ and $\hat{\Theta}_k(t)$ are of dimensions $\left(N_y+1\right)\times 1$, but boundary conditions are described by equation (12) and should be included in the positions y_0 and y_N, by the discretized boundary conditions. D_1 and D_2 are the Chebyshev differentiation matrices without the first and last row as in [35,p.89], whose elements are $d_{j,l}^{(1)}$ and $d_{j,l}^{(2)}$ respectively. This system of equations is solved after time discretization using the four-time level, third order temporal discretization procedure AB/BDI3. The semi-implicit methods apply generally to nonlinear equations such as (23) and (25) when the coefficient of the linear operator L(χ) is time-independent. This is the case for Navier-Stokes equations for incompressible fluids with constant viscosity. This linear term L(χ) is considered implicitly and the nonlinear term N(χ) is explicit, so that the resulting discrete operator is time-independent and can be inverted or diagonalized in a preprocessing stage performed before the start of time integration. The high order AB/BDIm (m=2,3,4) schemes involve the linear part L(χ) at time level n+1 only, and can be described by the following expression,

$$\frac{1}{\Delta t}\sum_{j=0}^{m}a_j\chi^{n+1-j}+\sum_{j=0}^{m-1}b_jN\left(\chi^{n-j}\right)=L\left(\chi^{n+j}\right), \tag{28}$$

where $\chi = \Psi_k(t)$, $\Omega_k(t)$, $\Theta_k(t)$. The values of the coefficient for AB/BDI3:

$$a_0 = \frac{11}{6}, a_1 = -3, a_2 = \frac{3}{2}, a_3 = -\frac{1}{3}, b_0 = 3, b_1 = -3, b_2 = 1. \tag{29}$$

The system is then reduced to a four-time level matrix system of equations for each wave-number $k = 0,1,...,K$, where $K = N_x/2$, which should be solved for each time step Δt. The equations after time discretization have the following form,

$$\left[\left(\frac{a_0}{\Delta t} + 4a^2k^2\,\mathrm{Pr}\right)\mathrm{I}_1 - 4\,\mathrm{Pr}\,\mathrm{D}_2\right]\hat{\Omega}_k^{n+1} + \frac{1}{\Delta t}\mathrm{I}_1\left(a_1\hat{\Omega}_k^n + a_2\hat{\Omega}_k^{n-1} + a_3\hat{\Omega}_k^{n-2}\right) = \hat{F}_{k,*}^{n+1},$$

$$\mathrm{I}_1\hat{\Omega}_k^{n+1} + 4\left(-a^2k^2\mathrm{I}_1 + \mathrm{D}_2\right)\hat{\Psi}_k^{n+1} = 0_1,$$

$$\left[\left(\frac{a_0}{\Delta t} + 4a^2k^2\right)\mathrm{I}_1 - 4\mathrm{D}_2\right]\hat{\Theta}_k^{n+1} + \frac{1}{\Delta t}\mathrm{I}_1\left(a_1\hat{\Theta}_k^n + a_2\hat{\Theta}_k^{n-1} + a_3\hat{\Theta}_k^{n-2}\right) = \hat{Q}_{k,*}^{n+1}, \tag{30-32}$$

$$\hat{\psi}_{kN}^{n+1}(y_0) = \hat{g}_{\psi+,k}^{n+1}, \quad \frac{\partial\hat{\psi}_{kN}^{n+1}}{\partial y}(y_0) = \sum_{l=0}^{N} d_{0,l}^{(1)}\hat{\psi}_{kN}^{n+1}(y_l) = \hat{h}_{\psi+,k}^{n+1}, \tag{33}$$

$$\hat{\psi}_{kN}^{n+1}(y_N) = \hat{g}_{\psi-,k}^{n+1}, \quad \frac{\partial\hat{\psi}_{kN}^{n+1}}{\partial y}(y_N) = \sum_{l=0}^{N} d_{N,l}^{(1)}\hat{\psi}_{kN}^{n+1}(y_l) = \hat{h}_{\psi-,k}^{n+1},$$

$$\hat{\theta}_{kN}^{n+1}(y_0) = \hat{g}_{\theta+,k}^{n+1}, \quad \frac{\partial\hat{\theta}_{kN}^{n+1}}{\partial y}(y_0) = \sum_{l=0}^{N} d_{0,l}^{(1)}\hat{\theta}_{kN}^{n+1}(y_l) = \hat{h}_{\theta+,k}^{n+1}, \tag{34}$$

$$\hat{\theta}_{kN}^{n+1}(y_N) = \hat{g}_{\theta-,k}^{n+1}, \quad \frac{\partial\hat{\theta}_{kN}^{n+1}}{\partial y}(y_N) = \sum_{l=0}^{N} d_{N,l}^{(1)}\hat{\theta}_{kN}^{n+1}(y_l) = \hat{h}_{\theta-,k}^{n+1}.$$

Here we use $N=N_y$ and the following matrices notation

$$\mathrm{I}_1 = \left[\delta_{i,j}\right], \quad \mathrm{D}_1 = \left[d_{i,j}^{(1)}\right], \quad \mathrm{D}_2 = \left[d_{i,j}^{(2)}\right], \quad i = 1,...,N-1, \quad j = 0,...,N,$$

$$\mathrm{I}_2 = \left[\delta_{i,j}\right], \quad \mathrm{D}_3 = \left[d_{i,j}^{(1)}\right], \qquad i = 0, N, \qquad j = 0,...,N. \tag{35}$$

If we introduce the following 2×1 column matices

$$G_{\psi,k}^{n+1} = \begin{bmatrix}\hat{g}_{\psi+,k}\\ \hat{g}_{\psi-,k}\end{bmatrix}^{n+1}, H_{\psi,k}^{n+1}, = \begin{bmatrix}\hat{h}_{\psi+,k}\\ \hat{h}_{\psi-,k}\end{bmatrix}^{n+1}, \quad G_{\theta,k}^{n+1} = \begin{bmatrix}\hat{g}_{\theta+,k}\\ \hat{g}_{\theta-,k}\end{bmatrix}^{n+1}, \quad H_{\theta,k}^{n+1} = \begin{bmatrix}\hat{h}_{\theta+,k}\\ \hat{h}_{\theta-,k}\end{bmatrix}^{n+1}, \tag{36}$$

and construct the following (N−1)×(N+1) matrices

$$\mathrm{B}_0 = \left(\frac{a_0}{\Delta t} + 4a^2k^2\,\mathrm{Pr}\right)\mathrm{I}_1 - 4\,\mathrm{Pr}\,\mathrm{D}_2, \quad \mathrm{B}_1 = \frac{a_1}{\Delta t}\mathrm{I}_1, \quad \mathrm{B}_2 = \frac{a_2}{\Delta t}\mathrm{I}_1, \quad \mathrm{B}_3 = \frac{a_3}{\Delta t}\mathrm{I}_1,$$

$$\mathrm{B}_4 = 4\left(-a^2k^2\mathrm{I}_1 + \mathrm{D}_2\right), \quad \mathrm{B}_5 = \left(\frac{a_0}{\Delta t} + 4a^2k^2\right)\mathrm{I}_1 - 4\mathrm{D}_2, \quad \mathbf{0}_1 = \mathrm{I}_1 0, \tag{37}$$

our system of equations for the Fourier coefficients obtains the following form

$$\mathrm{B}_0\hat{\Omega}_k^{n+1} + \mathrm{B}_1\hat{\Omega}_k^n + \mathrm{B}_2\hat{\Omega}_k^{n-1} + \mathrm{B}_3\hat{\Omega}_k^{n-1} = \hat{F}_{k,*}^{n+1}, \ \mathrm{I}_1\hat{\Omega}_k^{n+1} + \mathrm{B}_4\hat{\Psi}_k^{n+1} = \mathbf{0}_1,$$

$$\mathrm{B}_5\hat{\Theta}_k^{n+1} + \mathrm{B}_1\hat{\Theta}_k^n + \mathrm{B}_2\hat{\Theta}_k^{n-1} + \mathrm{B}_3\hat{\Theta}_k^{n-2} = \hat{Q}_{k,*}^{n+1},$$

$$\mathrm{I}_2\hat{\Psi}_k^{n+1} = G_{\psi,k}^{n+1}, \ \mathrm{D}_3\hat{\Psi}_k^{n+1} = H_{\psi,k}^{n+1}, \ \mathrm{I}_2\Theta_k^{n+1} = G_{\theta,k}^{n+1}, \ \mathrm{D}_3\hat{\Theta}_k^{n+1} = H_{\theta,k}^{n+1}. \tag{38-44}$$

The initial conditions read

$$\psi(x,y) = 0, \quad \omega(x,y) = 0, \ T(y) = \frac{1}{2}(1-y), \ 0 \le x \le 2\pi, \ -1 \le y \le 1, \quad t = 0,$$

$$Ra_p(t) = Ra_p\sin(t), \quad Ra_{uni}(t) = Ra_{uni}\sin(t), \ \gamma = 0, \quad 0 \le t \le \pi/2,$$

$$Ra_p = 30, \quad Ra_{uni} = 500, \ \gamma^{n+1} = \gamma^n + \Delta\gamma, \quad 0 \le \gamma \le 20\pi/180, \quad \pi/2 \le t \le \pi. \tag{45}$$

The Fourier-Galerkin spectral method gave an accurate spatial resolution with $K = N_x/2 = 64$, $N_y = 128$ Gauss-Lobatto-Chebyshev points, and for temporal discretization we used time step

$\Delta t = \pi/300$, the angle of inclination increment $\Delta\gamma = 20\pi/180 \cdot 1/150 = \pi/1350$. All results presented in this paper were obtained with an accuracy of at least four digits.

4. Numerical Results

Equations (38-40) with boundary (41-44) and initial (45) conditions were solved numerically by using the influence matrix method and the numerical code developed in MATLAB. The validation of numerical results was done by carrying out numerical simulation for the values of Ra_{uni}=0, Ra_p=400, shown in fig.(6) in [37] and figs.(4,7-9) in [38] for several different values of Q, but not the same geometry. Our results for ψ_{max} do not differ from these results for more than 2%.

We can see the dimensionless vorticity, stream function, and temperature for subcritical Rayleigh numbers $Ra_{uni} = 500$, $Ra_p = 30$, aspect ratio $a = 1$, where the critical value for this flow is $Ra_{cr} = 1708$ for the wavenumber of disturbance $q_{cr} = 3.16$. So, for this value of Ra_{uni} there should not be any flow, if there were uniform temperature distribution at the lower wall (if $Ra_p = 0$). Fig.2 shows these three scalar fields for three different angles of inclination $\gamma = 0$, $10\pi/180$, $20\pi/180$ at the instant of time $t = \pi/2$, $3\pi/4$, π, respectively. The wavenumber of periodic temperature distribution at the lower plate is $\alpha = 2$ for this simulation, and there is no temperature phase shift $(\varphi = 0)$ on the lower wall. *Hot spots*, locations where periodic temperature on the lower plate attains its maximum, are located at $x^* = 0, \pi, 2\pi$, and *cold spots* positions where the periodic component of temperature attains its minimum are located in $x^* = \pi/2$, $3\pi/2$, in accordance with the temperature distribution given by (12) and periodic temperature wavenumber $\alpha = 2$ on the lower wall. In the instant of time $t = \pi/2$, when $\gamma = 0$, Ra_p and Ra_{uni} attain their maximal values according to equation (44), and they remain constant for $t > \pi/2$. In fig.2 (a,c,e)-left column, where the dimensionless vorticity distribution $\omega(x, y, t)$ is displayed, we can see two pairs of vortexes which rotate in the clockwise (blue area) and counterclockwise directions (orange area). Just above these *hot spots*, the fluid motion is directed upwards, hits the upper cooler surface, splits into two streams parallel with plates, gets cooled and its density gets higher and then drops from the upper to the lower plate at $x^* = \pi/2$, $3\pi/2$ in *cold spots*, where the temperature achieves its minimum according to (12). The fluid rises above the *hot spots* and descends toward the *cold spots* forming counter-rotating rolls displayed as streamfunction in fig.2 (b,d,f). The nondimensional vorticity intensity $\omega(x, y, t)$ can be compared for three different inclination angles $\gamma = 0$, 10°, 20°, at the corresponding instant of time $t = \pi/2$, $3\pi/4$, π respectively, see fig.2 left column, after the periodic Rayleigh number achieves its value $Ra_p = 30$ and $Ra_{uni} = 500$ at the instant of time $t = \pi/2$.

Two pair of vortexes rotate with the same intensity for $\gamma = 0$, displayed in fig.2(a), but in the opposite direction, clockwise-negative direction (blue color) and counterclockwise - positive direction (orange color), and the extreme values of vorticity are $\omega_{max}(2.344, -0.049) = 54.31$, $\omega_{min}(3.913, -0.049) = -54.31$. The borders between vortexes overlap with the peaks and bottoms of fluid temperature distribution depicted in fig.3(a), which also overlap with the hot and cold spots on the lower wall. But for $\gamma = 10°$ $(t = 3\pi/4)$, fig.2(c) the same pair of vortexes has altered its vorticity to the values $\omega_{max}(1.865, -0.049) = 46.58$, $\omega_{min}(3.424, -0.049) = -58.88$. We can see that the orange color vortex decreases its intensity of angular momentum, and the blue color roll increases its magnitude of rotation between these two instant of time $t = \pi/2$ and $t = 3\pi/4$, i.e. between the two inclination angles $\gamma = 0$ and $\gamma = 10°$. The displacement of their centers in the negative x-direction is not the same, because

one of them shrinks and the other one expands in the x-direction, as it will be seen on fig.2(b,d,f) for streamfunction and much clearer in fig.3(b,d,f) for streamlines distribution.

This tendency continues for the higher values of the inclination angle, so for $\gamma = 20°$ and $t = \pi$, fig.2(e) we $\omega_{\max}(0.491,-0.098) = 20.65$, $\omega_{\min}(2.074,0.00) = -56.43$. We see that the counterclockwise rotating roll (orange one) gets weaker, loses its intensity of rotation and shrinks in the x-direction, but the clockwise (blue one) rotating vortex gets stronger, increases its magnitude of vorticity and extends in the x-direction with the increasing angle of inclination γ. For the angle $\gamma = 20°$ and time $t = \pi$ fig.2(e) we can notice that minimal vorticity $\omega_{\min}$ declines in its absolute value with respect to value at $\gamma = 10°$ and time $t = 3\pi/4$. In the same fig.2 (a,c,e), we can see that besides the existing main two vortex pairs in the middle of the slot, there exist two vortexes with the opposite sign on the upper and lower wall just above and below the rolls (central vortex) considered. These small vortexes on the walls change its magnitude depending on the inclination angle γ, too. Two positive small vortexes, above and below the clockwise rotating central vortex in the middle of the slot, increase its magnitude together as the clockwise rotating central vortex increases its absolute value. The two negative small vortexes on the walls, above and below the counterclockwise rotating central vortex, decrease their intensity as the magnitude of central positive vortex decreases its magnitude with the increasing inclination angle γ. The position of these small vortexes on the upper and lower wall moves in the direction of the negative x-axis with rising γ, and is fixed with respect to the central vortexes in the middle of the slot. The position of these small wall vortexes is *locked in* with the position of central vortexes, and is located just above and below them. These values on the lower plates for $\gamma = 0$ are $\omega_{maxL}(x=3.866,y=-1,t=\pi/2)=46.92$, and in the middle of the slot $\omega_{maxM}(x=5.473,y=0,t=\pi/2)=54.63$. Further we can notice the same tendency, where the maximal values of vorticity on the lower plate and in the middle of the slot have the following values for $\gamma = 10°$ $\omega_{maxL}(x=3.375,y=-1,t=3\pi/4)=56.65$, $\omega_{maxM}(x=5.00,\ y=-0.024,\ t=3\pi/4)=46.57$, and finally we obtain for $\gamma = 20°$ the vorticity $\omega_{maxL}(x=1.939,y=-1,t=\pi)=60.14$,$\omega_{maxM}(x=3.632,\ y=-0.098,\ t=\pi)=20.65$. We can conclude that the maximal vorticity in the middle slot of counterclockwise rotating vortexes declines rapidly and these positive vortexes shrink, but the maximal vorticity in the wall positive vortexes climbs slowly and achieves the asymptotic value at $\omega_{maxL}(\gamma=20°)=60.14$.

This could be explained by the fact that with the rising inclination angle γ the fluid that ascends from the hot spot hits the upper plate and splits into two equal streams if $\gamma=0$, and into two unequal streams if $\gamma\neq 0$. In our case for $\gamma>0$ the greater amount of hot fluid streams upwards beneath the upper plate in the positive direction of the x-axis, and a smaller amount of hot less dense fluid streams downward, beneath the upper plate in the negative direction of the x-axis, and this tendency is more pronounced with the rising angle of inclination γ. We obtained these results but because of limited space in this paper, these fields of velocity components are omitted. The results for the u-velocity component, clearly indicates that the balance between the positive and negative values of the u-velocity component at $x=\pi$, $y=1$ which exists for $\gamma=0$, is compromised for the case $\gamma>0$, and for increasing γ this misbalance is more pronounced in favor of the positive values of the u-velocity component. The amount of fluid, which enters the clockwise rotating roll right after hitting the upper wall, increases with rising γ, so the central negative roll extends, but since the smaller amount of fluid goes downwards left beneath the upper plate and enters the counterclockwise-rotating roll, this roll shrinks, see fig.2(b,d,f) and more clearly fig.3(b,d,f). Afterwards, the strength of these central rolls is not equal any more, and the strength of the clockwise-rotating rolls increases and the strength of the

counterclockwise-rotating rolls decreases, as shown in fig.2(b,d,f). The explanation for such behavior could be explained by the result of the formation of a non-zero component of the buoyancy force that acts along the *x*-axis direction.

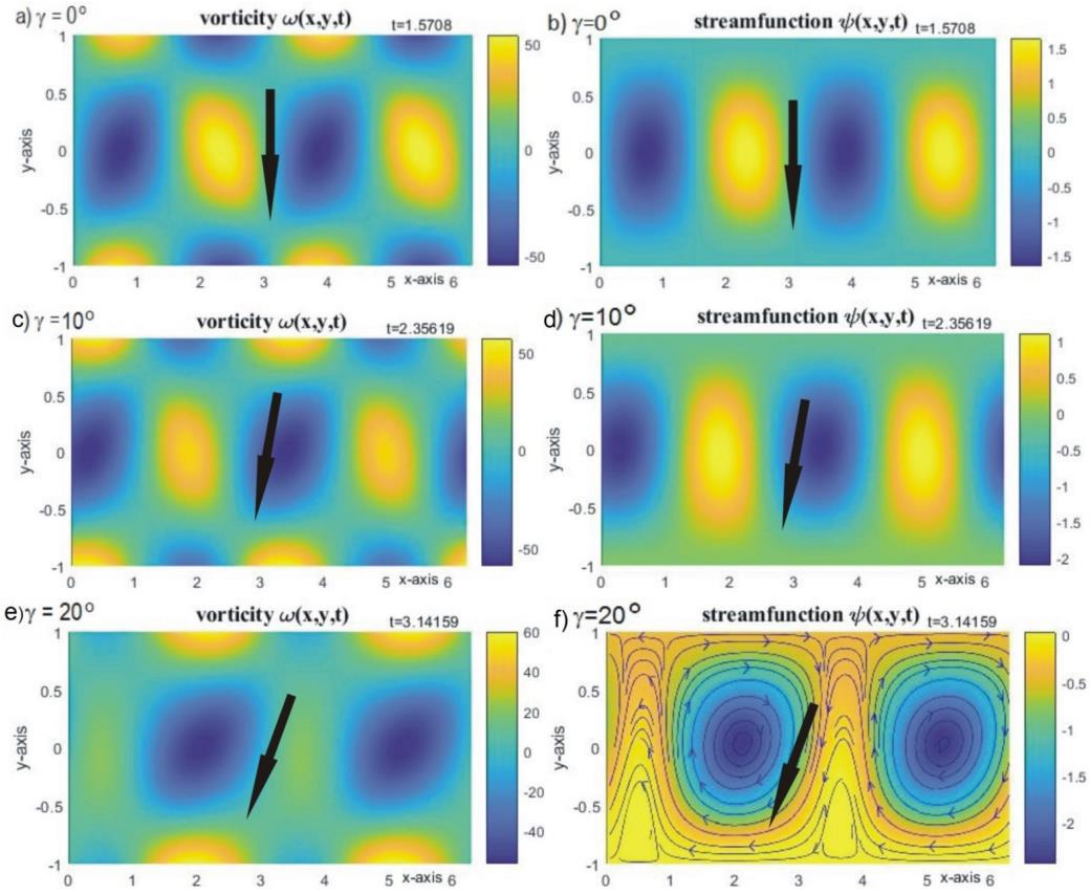

Figure 2. Distribution of vorticity, stream function, for Pr=7 for inclination angles γ=0,10°,20°.

One can interpret this process as a hot plume impacting an oblique upper flat plate. Some of the fluid is permanently trapped inside the rolls while the reminder travels along the slot. The cumulative net flow is a function of both the inclination angle and the heating intensity and it seems that positive rotating rolls significantly weaken as the inclination angle increases. Indeed, we note that the counterclockwise rotating rolls were completely washed away once the inclination angle reaches γ>20°. The fact that both component of buoyancy force differ from zero at some γ>0°, since its curl is defined as $\nabla\times\vec{F}=\left(\partial F_y/\partial x-\partial F_x/\partial y\right)\vec{k}$, has the impact on vorticity redistribution inside the slot. The curl of force term in vorticity transport equation is defined as the limit of circulation to the area as the area tends to zero. As the gradients difference in $\nabla\times\vec{F}$ becomes greater in some points in the domain, i.e. in the points close to walls for counterclockwise rotating rolls the vorticity gets stronger. The same is valid for clockwise rotating rolls in the middle of the slot. Since the components of buoyancy force are dependant on temperature Eq.(6), its temperature gradients and inclination angle determine the vorticity distribution inside the slot. As the fluid starts sliding downward for γ>0°,these gradients become stronger, and the magnitude of vorticity increases but to some limiting value in our case γ=20°. After this angle the fluid flow is not structured any more. *Thermal drift* becomes evident at higher values of γ, in our case it is obvious in fig.3(f) and in the case of streamlines plotted together with stream function for γ=20°at t=π or in fig.2(f). During this process of increasing the inclination angle γ with time, the centers of rolls move in the direction of the negative *x*-axis, and the center of

counterclockwise rotating rolls moves also in the direction of the negative *y*-axis, in the direction closer to the lower wall. The distance Δx between the center position of two positive rotating rolls at $\gamma=0$ and the position when $\gamma>0$ is increased.

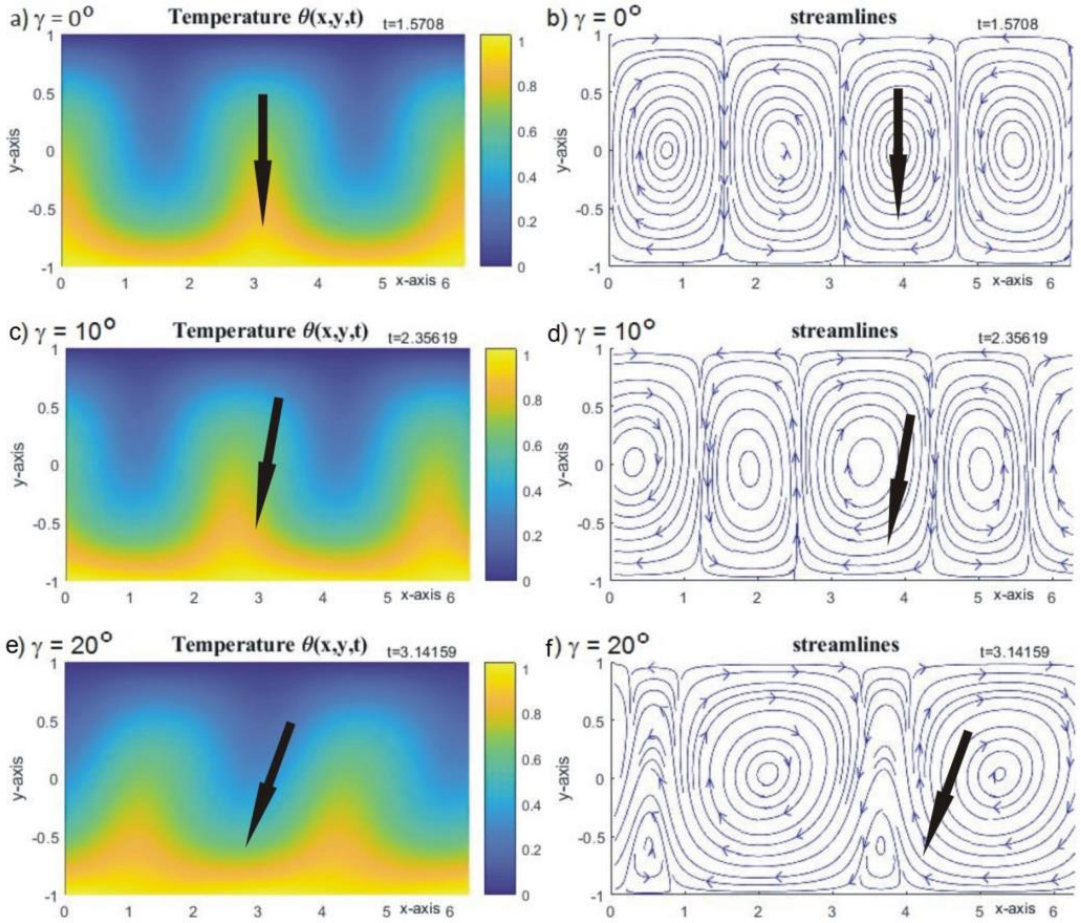

Figure 3. Distribution of temperature and streamlines for five angle of inclinations γ=0°,10°,20°.

With increasing Δx, the phase shift φ_f between fluid temperature pattern and the periodic temperature distribution on the lower plate increases, and attains its highest value at $t=\pi$, ($\gamma=20°$). The displacement of roll centers for this time period is $\Delta x=x_5-x_1=2.086-3.783=-1.697\approx-\pi/2=\varphi_f$, and it causes the flow pattern *phase shift* between the *locked in* fluid flow pattern [36] and the periodic temperature pattern on the lower plate, which results in the appearance of *thermal drift*, described in [37-39] for the case of the phase shift φ between two sinusoidal functions applied to the lower plate temperature and corrugation distribution. In our case, practically φ_f is a *phase shift* between hot spots in the periodic temperature distribution on the lower wall and the fluid temperature tips. This is a consequence of the negative nondimensional volumetric flow rate $\psi(y=1)<0$, and the displacement of fluid flow pattern in the negative direction of the *x*-axis if there exists some positive inclination angle $\gamma>0$. The centers of the positive counter-rotating rolls are shifted toward the lower wall when $\gamma>0$, and this can be noticed for $\gamma=20°$, when the center of the positive diminishing roll is moved significantly to the lower wall, as can be seen in fig.2(f) for ψ_{max} ($x=3.62, y=-0.67, t=\pi$)=0.03795. The results displayed in fig.2(b,d,f) for streamfunction ψ_{max} (x,y,t) demonstrate that the position of the roll centers remain constant with respect to the *y*-axis for low values of the inclination angle γ, and once when certain value $\gamma=10°$ is reached, the counterclockwise (positive) rotating roll centers start moving downward

and go away from the center of the slot for higher values of γ>10°. However, in the same time period these rolls shrink, decrease their width and height, and weaken the strength of the rolls.

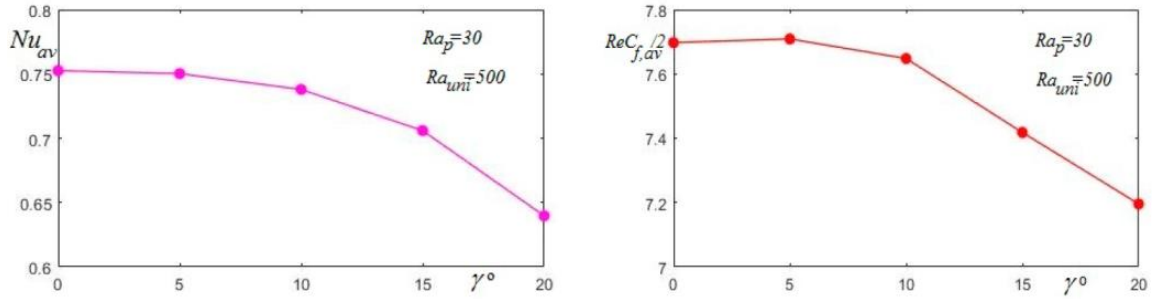

Figure 4. Distribution of Nusselt average number Nu_{av} and average friction coefficient $C_{f,av}$ multiplied by Re/2 for five different angle of inclination γ=0,5°,10°,15°,20°.

Fig.4 shows the Nusselt and skin friction coefficient average number as a function of γ. We can see that both of them have a tendency to decline with the increasing inclination angle γ. Both values have been calculated for the lower plate, where the Nusselt number is displayed in the absolute value, since its values on the lower plates have a negative sign. This can be explained by the fact that thermal energy goes from the lower to the upper plate, and the lower one loses and the upper one gains thermal energy. This results are in accordance with the results presented in [33,40,41].

5. Conclusions

We have discussed the response of a system that combines uniform and periodic heating components in a slot that starts tilting with respect to time. We can notice that the intensity of counter-clockwise rotating central vortexes in the middle of the slot declines with the increasing γ, and the magnitude of clockwise rotating small vortexes on the upper and lower wall just above and below this central positive vortex also descends with the increasing inclination angle γ. The opposite is also true, the magnitude of clockwise rotating central vortexes in the middle of the slot increases with the rising angle γ, and the magnitude of counterclockwise rotating small vortexes on the upper and lower wall just above and below this central negative vortex also ascends with the increasing inclination angle γ.This can be demonstrated by comparing positive rotating vortexes on the walls and in the middle of the slot.

If the hot spots overlap with the tips of the fluid flow temperature distribution, convection takes on the shape of counter rotating rolls, which come in pairs and whose size is determined by the heating wavelength. The formation of the *stream tube*, is found in all other relative positions occupied by the hot spots and the fluid flow temperature tips. This stream tube is formed in the presence of both the periodic heating on the lower plate and the periodic fluid temperature distribution which slides down due to inclination and gravity component in *x*-axis induced flow, and it can then be directed, depending on the phase difference φ_f between the periodic heating and the fluid flow temperature distribution, in the positive as well as in the negative *x*-axis flow direction. In our case it depends on the negative or positive values of inclination angle γ, whether the component of gravitational acceleration in the direction of the *x*-axis is positive or negative, and stream tube is a very strong function of phase difference, in our case the largest stream tube occurred for inclination angle γ=20° at the instant of time t=π. If γ≠0 the fluid temperature pattern starts sliding in the direction of the gravity component parallel to the *x*-axis. For the case of γ>0 it is in the negative, and for γ<0 it is in the

positive direction of the *x*-axis. Fig.2 and fig.3 show patterns for phase shifts $\varphi_f = 0,\ldots,\pi/2$, with the flow topology comprising sets of rolls separated from each other by a stream tube weaving up and down and carrying fluid in the negative *x*-direction, for our case $\gamma > 0$.

Acknowledgment

The paper is a part of the research done within the project of Faculty of Mechanical Engineering in Niš, financially supported by the Ministry of Education, Science and Technological Development of the Republic of Serbia (Contract No.451-03-9/2021-14/200109).

References

[1] Rayleigh J.W.S. "On convection currents in a horizontal layer of fluid, when the higher temperature is on the under side". *Phil. Mag. vol.32* (1916), pp. 529-546.

[2] Bénard H., "Les tourbillons cellulaires dans une nappe liquide". *Revue Générale Science Pure et Applique, vol.11* (1900) , pp.1261-1271.

[3] Bodenschatz E., *et al.*, "Recent developments in Rayleigh-Bénard convection" *Annual Review of Fluid Mechanics, vol.32* (2000),, pp.709-778.

[4] Chilla F., Schumacher J., "New perspective in turbulent Rayleigh-Bénard convection" *Eur. Phys. J., E 35* (2012), pp.58-82.

[5] Hassanzadeh P.,*et al.*,"Wall to wall optimal transport", *J. Fluid Mech., vol.751* (2014),621-662,.

[6] Clever R.M., Busse F.H., "Transition to time-dependant convection", *J. Fluid Mech., vol.65* (1974), pp.625-645.

[7] Busse F.H., Clever R.M, "Instabilities in convection rolls in a fluid of moderate Prandtl number". *J. Fluid Mech., vol.91* (1979), pp.319-335.

[8] Ahlers G *et al.*, "Heat transfer and large scale dynamics in turbulent Rayleigh-Bénard convection", *Rev. Mod. Phys., vol.81* (2009), pp.503-537.

[9] Lohse D., Xia K.Q.,"Small scale properties of turbulent Rayleigh-Bénard convection". *Annu. Rev. Fluid Mech. , vol.42* (2010), pp.335-364.

[10] Toppaladoddi S., *et al.*,"Tailoring boundary geometry to optimize heat transport in turbulent convection*". Eur. Phys. Lett. A*, vol. 111 (2015), 44005.

[11] Golushkin D., Doering C.R.,"Bounds for convection between rough boundaries", *J. Fluid Mech., vol.804* (2016), pp.370-386.

[12] Mc Coy J.H., *et al.*, "Self-organization of topological defects due to applied constraints", *Phys. Rev. Lett., vol.101* (2008), 254102.

[13] Seiden G., *et al.*,"Pattern forming system in presence of different symmetry-breaking mechanism", *Phys. Rev. Lett., vol.101* (2008), 214503

[14] Weiss S., *et al.*,"Pattern formation in spatially forced thermal convection", *New J. Physics, vol.14* (2012), 053010.

[15] Abtahi A., Floryan J.M.,"Natural convection in a corrugated slots" *J.Fluid Mech.*,vol.815 (2017), pp.537-569.

[16] Freund G., *et al.*,"Rayleigh-Bénard convection in the presence of spatial temperature modulation", *J. Fluid Mech., vol.673* (2011), pp.318-348.

[17] Hossain M.Z., *et al.*, "Drag reduction due to spatial thermal modulation" , *J.Fluid Mech., vol.713* (2012), pp.398-419.

[18] Hossain M.Z., Floryan J.M.,"Mixed convection in periodically heated channel", *J.Fluid Mech.,vol.768* (2015a), pp.51-90.

[19] Hossain M.Z., Floryan J.M., "Natural convection in horizontal fluid layer periodically heated from above and below".*Phys. Rev., E92* (2015b), pp.02301

[20] Hossain M.Z., Floryan J.M., "Natural convection under sub-critical conditions in the presence of heating non-uniformities". *Int. J. Heat and Mass Transfer, vol.114* (2017), pp.8-19.

[21] Hossain M.Z., Floryan J.M.,"Instability of natural convection in a periodically heated layer*".J. Fluid Mech., vol.733* (2013), pp.33-67.

[22] Zhao C., *et al.*, "Suppression of flow reversals via manipula-ting corner rolls in plane Rayleigh–Bénard convection*". J. Fluid Mech.,vol.946*, (2022), A44.

[23] Zhao C., *et al.*, "Modulation of turbulent Rayleigh-Benard convection under spatially harmonic heating". *Physical Review E, 105*, (2022) 055107.

[24] Vanishree R.K.,Anjana K.,"The Linear and Non-linear Study of Effects of Temperature Modulaton on Double Diffusive Convection in Oldroyd-B Liquids". *Int.J.Appl.Comput.Math vol.3*, suppl.1, (2017), p.1095-1117,

[25] Chen X., *et al.*,"Nusselt number influenced by expansion/compression, birth/death, and recirculating direction of vortices in elongated enclosures". *Inter.Commun.Heat and Mass Transfer, vol.97*, (2018), p.110-117.

[26] Jovanović M.M., *et al.*, "Rayleigh-Benard convection instability in the presence of spatial te-mperature modulation on both plates", *Inter. J. Non-Linear Mech, vol.73* (2015), pp.69-74.

[27] Petrovic J.D., et.al.,"MHD flow and mixed convection of viscous fluid and a nanofluid through a porous medium in a vertical channel." https://doi.org/10.2298/TSCI:220903188P,online first only,

[28] Cheong H., *et al.*,"Effect of aspect ratio on natural convection in an inclined rectangular enclosure with sinusoidal boundary condition", *Intern.Comm.in Heat and Mass Transfer, vol.45* (2013), pp.75-85.

[29] Floryan J.M., *et al.*, "Natural convection and pattern interaction in a two-dimensional vertical slot", *J. Fluid Mech., vol.946*, (2022), A20.

[30] Siggers J.H., *et al.*, "Bounds on horizontal convection". *J. Fluid Mech. 517* (2004), pp. 55-70.

[31] Hossain M.Z., Floryan J.M., "Heat transfer due to natural convection in a periodically heated layer", *ASME J.Heat Transer,135*, (2013b), 022503.

[32] Ehrenstein U., Peyret R., "A Chebyshev collocation method for solving Stokes-type equations." In Bristeau, et.al. (eds), *Proceedings*: Sixth Int.Symp.Finite Elements in Flow Problems. INRIA, 1986, pp. 213-218.

[33] Floryan J.M.,Baayoun A.,"Pattern convection in inclined slots",*J.Fluid Mech.,950,*(2022), A11.

[34] Peyret R., Krause E., *Advanced turbulent flow computations*, CISM courses and lectures N.395, Springer Verlag Wien, 2000.

[35] Canuto C., Hussaini M.Y., Quarteroni A., Zang T.A., *Spectral Methods*, Fundamentals in Single Domain, Springer Verlag, New York, 2007.

[36] Hossain M.Z., Floryan J.M., "Wavenumber lock in and spatial parametric resonance in convection", *J. Fluid Mech., vol.944*, (2022),A47.

[37] Abtahi A., Floryan J.M., "Natural convection and thermal drift", *J. Fluid Mech. vol.826* (2017), pp. 553-582.

[38] Abtahi A., Floryan J.M.,"On the formation of thermal drift", *Phys. Fluds,30,(4),* (2018), 043602.

[39] Inasawa A., Hara .K., *et al.*, "Experiments on thermal drift" *Phys.Fluids, 33(8),* (2021), 087116.

[40] Hossain M.Z., Floryan J.M., “On the role of surface grooves in the reduction of pressure losses in heated channels”. *Phys. Fluids, vol.32* (2020), 083610.

[41] Floryan J.M., *et al.*, “Heating induced drag reduction in relative movement of parallel plates”. *Phys.Rev.Fluids, vol.3* (2018),

Paper submitted: 27.04.2023
Paper revised: 29.06.2023
Paper accepted: 12.07.2023